Connecting Spatial Variability in Surface Forcing and Boundary Layer Height with a 1D Advection-Resolved Model in CHEESEHEAD19

M.P. van Soest

Supervisors: Ankur Desai, Paul Stoy (UW Madison), Aarnout van Delden (Utrecht University)

May 23, 2022

Abstract

The prediction of the boundary layer height (BLH) and understanding of its interactions with the earth's surface is vital for air quality control, climate modelling and weather prediction. The modelling of processes in the boundary layer has improved to have resolutions in the 'terra incognita', where energy-containing eddies are partially being resolved. In this study a simple 1D model that predicts BLH based on observed surface fluxes is coupled to a 2D advection scheme mixing the BLH over the CHEESEHEAD19 domain using the mean wind. BLH variability caused by surface flux variability is found on scales of 1 km and the influence is dampened by increasing wind speed. The model produces realistic predictions of BLH, which are within 100 m from from observations for clear days and more than 500 m from observed values for cloudy days, which shows that the model assumptions do not hold in conditions with high wind speeds, wind shear or horizontal divergence. The model should be further validated using observations or LES model results and improvements could entail subsidence, flux footprints and an implementation of the cloud feedback.

1 Introduction

The atmospheric boundary layer (ABL) is the lowest layer of the atmosphere, typically reaching a depth of 1-2 km during the day. Since it is the layer we live in and because of its interactions with the earth's surface, the prediction and understanding of the ABL is vital for air quality control, [Li et al., 2017], climate modelling and weather forecasting [Edwards et al., 2020a].

The modelling of the boundary layer height (BLH) is at an interesting stage of development. In the past, meteorological models have always had a resolution far coarser than the size of the energy containing eddies in the boundary layer, which means these processes have had to be parameterized. The models that do fully resolve the eddies in the boundary layer, using Large Eddy Simulation (LES), have a resolution much smaller than the size of the energy-containing eddies but therefore cannot be applied to the entire planet. Over the past years, global climate models and weather prediction models have been developed with a horizontal resolution approaching 1 km. This means that the assumption that the resolution is much larger than the size of the eddies no longer holds [Wyngaard, 2004]. The region of modelling with resolution around the size of energy containing eddies, which is between the coarse and fine resolution was dubbed by Wyngaard as the 'terra incognita' and is sometimes referred to as the 'grey zone'. Much research is being done now on possible ways to handle turbulence in this grey zone, since most of the turbulent eddies exist in this 'terra incognita' (figure 5 in Prein et al. [2015]). Modelling at these mesoscale resolutions means eddies get partially resolved but the energy transfer to smaller scales does not. The modelling of the BLH is particularly difficult in this regard because it grows from a night-time stable layer on the scale of 10 m to a deep and unstable layer on the scale of 1 km, thereby entering the grey zone [Kealy et al., 2019].

One solution to suppress turbulent motions being resolved is to use a 1D BLH scheme, such as the one by Lock et al. [2000] who used a classification of unstable layers and explicit entrainment parameterization or the one by Porporato [2009] and Gerken et al. [2018] for constant Bowen ratio. Several other studies, mainly focused on the effects of land treatments and agriculture, use extremely simple 1D parameterizations of boundary layer growth to study the effect of different types of land cover on local weather and climate [Vick et al., 2016] [Luyssaert et al., 2014].

Several studies have also highlighted the importance of different atmospheric conditions on the applicability of various boundary layer schemes [Edwards et al., 2020b], especially in climate models [Bony and Dufresne, 2005]. Sedlar et al. [2022] used a cloud regime classification model to separate the CHEESEHEAD19 days into 3 cloud classifications and found differences in boundary layer growth and importance of different factors in this process, suggesting cloud feedbacks in the interaction between land and atmosphere.

Since the boundary layer is strongly influenced by the surface, heterogeneities in the earth's surface can have a significant influence on our prediction and understanding of the processes in the boundary layer [Helbig et al., 2021]. A key aspect of the ongoing research is the measurement of surface fluxes. The first measurements by flux towers were published around 1970. Since then, flux towers have been set up all over the world and are now being combined by a in FluxNet: A worldwide network of flux towers that provide multi-year data from all over the world. Helbig et al. [2021] provide a review of the current state of land-atmosphere interaction research and emphasize the value of co-located flux-measurements with types other data assimilation. Many flux towers in a small domain is exceptional and provides a source of data that can be used to investigate the translation of surface flux heterogeneities to the BLH. The CHEESEHEAD19 field study provides a wealth of observations, with 17 flux towers, ground measurements, balloon sounding and cloud lidar measurements in a domain of 10 km x 10 km.

The models mentioned above are purely 1D, and for studying surface heterogeneities and 3D motions a horizontal component should be included. The approach chosen in this research is based on Desai et al. [2006], who used a 1D model to calculate the BLH and then treated the atmosphere as columns that mix with the wind, thereby diffusing the BLH. This rests on the assumption that the vertical response to the surface forcing happens on longer timescale than the advection and that the diffusion happens equally on all levels in the ABL. If the wind speeds are high or there is high wind shear or horizontal divergence, these assumptions become invalid and the model does not capture the horizontal mixing of the BLH. Adding advection in one direction improved the prediction of BLH in the case studied by Desai et al. It was also shown that heterogeneities in the depth of the boundary layer due to surface fluxes on scales of 100 km existed and suggested the same phenomenon on smaller scales, which would be in the terra incognita.

The goal of this study is to create a 1D advection-resolved model that predicts the BLH in the CHEESEHEAD19 domain using flux tower observations. The research questions that are investigated using this model are:

- Are surface heterogeneities imprinted on the BLH in the 'terra incognita' and what variables influence this process?
- How well does a 1D BLH model with a 2D advection scheme reproduce the BLH and does this depend on the cloud conditions?

First, the theoretical background of boundary layer growth is discussed in section 2, after which the used data is presented in section 3 and the model equations are introduced in section 4. Then, the results are shown in section 5. Finally, a discussion of the results is given in section 6 after which conclusions are drawn in section 7.

2 Theory

2.1 Atmospheric Boundary Layer

The atmospheric boundary layer (ABL) is the lowest part of the atmosphere and therefore is the part that is directly influenced by the earth's surface (ocean or land). The ABL is generally assumed to be perfectly mixed, meaning it has constant temperature, humidity and aerosol concentration. The top of the ABL is characterized by a stable layer that caps the turbulence in the ABL and has a strong temperature inversion and decrease of aerosol concentration, often referred to as the capping inversion [Garratt, 1994].

2.1.1 Dynamics

The state of the ABL is determined by exchanges of heat, momentum and scalars such as moisture, aerosols, methane and CO2. These variables are exchanged between the ABL, the surface and the free troposphere above the capping inversion [Helbig et al., 2021]. The interaction between these three layers, combined with the diurnal cycle of radiation, forms a complex system that consists of multiple feedback loops. This system is often referred to as Local Land-Atmosphere Coupling (LoCo), described in detail by Santanello Jr et al. [2011]. Van Heerwaarden et al. [2009] identify 3 main feedback loops in this coupling, shown schematically in figure 1.

The first feedback is concerned with heating, which is forced initially by radiation reaching the surface, causing both evaporation of water from the surface and sensible heating of the surface which in turn heats up the ABL. Through entrainment of heat with the free troposphere, the height of the ABL is increased by this feedback too. The heating of the ABL also causes a larger water deficit, increasing latent heating and thereby decreasing sensible heating.

Feedback 2 is the moisture feedback, which decreases the evaporation from the surface when the ABL moisture content rises, because the gradient between land and atmosphere drops. This feedback is negative since latent heating causes the atmosphere to moisten, which in turn lowers latent heating.

The third feedback described by van Heerwaarden et al. is the drying feedback. The sensible heat flux from the surface causes heating and therefore deepening of the ABL through entrainment of (usually) dry air. The dry air from the free troposphere decreases the ABL moisture, which in turn causes a lowering of sensible heating through an increase in latent heating.

These 3 processes give a rough picture of the surface-ABL-troposphere interaction, but are determined by many factors such as surface properties: vegetation type, soil moisture, soil temperature, vegetation structure and the state of the free troposphere, which can be influenced by large scale atmospheric processes.

Through radiative forcing and the system described here, the ABL growth and decays in a diurnal cycle. At sunrise it starts growing, after which it typically stabilizes in the afternoon when the negative feedbacks described above cause the ABL to reach constant temperature. When the sun sets, the heat flux driven turbulent mixing ceases, the daytime ABL collapses and a much shallower, stable boundary layer forms, with a residual layer above it.

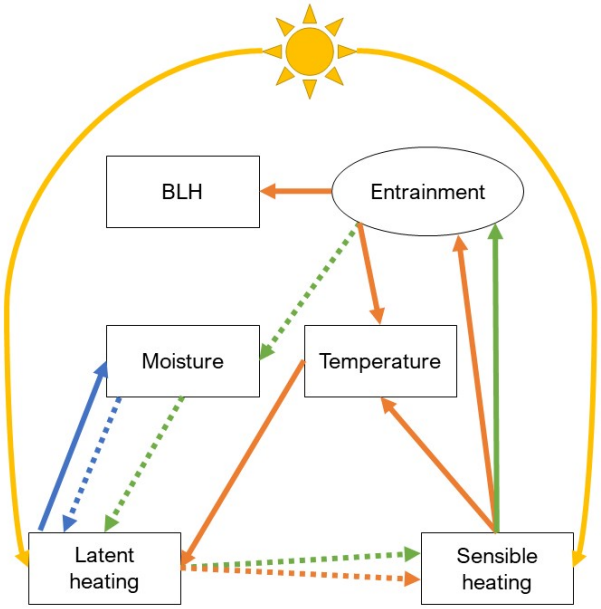

Figure 1: *Schematic of feedbacks working in boundary layer dynamics. Orange arrows represent the heating feedback, blue arrows represent the moisture feedback and green arrows represent the drying feedback. Solid arrows are positive relationships and dashed arrows are negative relationships. Yellow arrows are solar radiation. Recreated from Van Heerwaarden et al. [2009]*

3 Data

The Chequamegon Heterogeneous Ecosystem Energy-Balance Study Enabled by a High-Density Extensive Array of Detectors 2019 (CHEESEHEAD19) is a field study that has the goal of studying the response of the ABL to heterogeneities in surface energy fluxes. For this purpose, a large field-campaign was set up in 2019 in a forested region in Northern Wisconsin, centered around a 447 m tower containing an AmeriFlux/NOAA supersite (US-PFa/WLEF). In a 10 km x 10 km domain around this tower, 19 flux-measurement towers were set-up, as well as airborne and profiling instrumentation and surface environment characterization. The tower names and their environments are given in table 1. An extensive description of the study can be found in Butterworth et al. [2021]. The ecosystem in that area consists of different types of forests, grasslands, wetlands and open water. A map of the area is shown in figure 2.

In this research, the flux tower measurements of sensible and latent heat flux and surface temperature, pressure and humidity were used. Also, the balloon soundings done during the intensive observation periods (IOP's) at NW5 (ISS) were used to initialize and validate the model and the wind speeds and direction from the wind profiler at NW5 (ISS) were used for the advection scheme.

Tower	Type	Tower	Type
WLEF (Tall Tower)	Mixed wetland	NE4	Conifer
NW1	Conifer	SW1	Hardwood Deciduous
NW2	Hardwood Deciduous	SW2	Hardwood Deciduous
NW3	Tussock	SW3	Hardwood Deciduous
NW4	Lake	SW4	Hardwood Deciduous
NW5 (ISS)	Grass	SE2	Hardwood Deciduous
NE1	Conifer	SE3	Hardwood Deciduous
NE2	Conifer	SE5	Hardwood Deciduous
NE3	Hardwood Deciduous	SE6	Conifer

Table 1: *Information on the flux towers and their environments.*

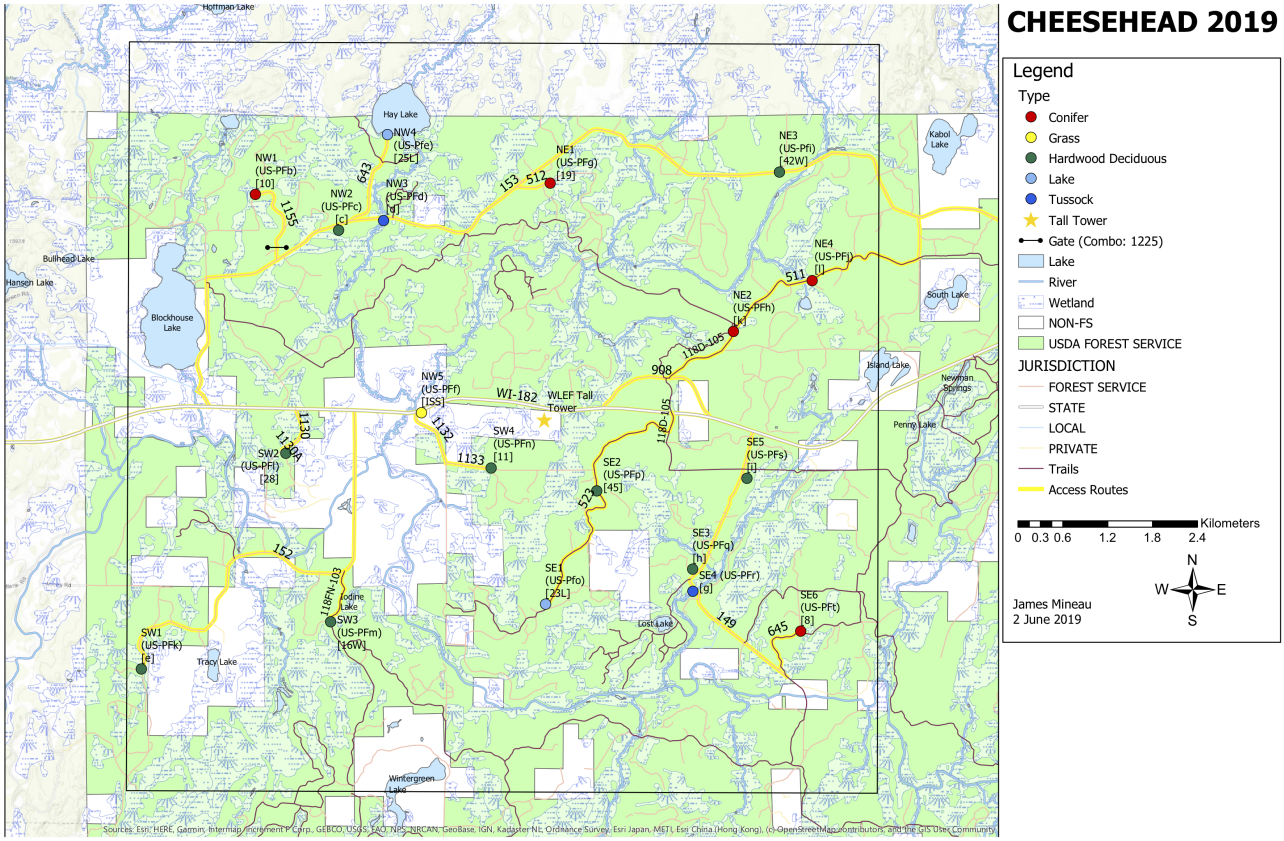

Figure 2: *Map of the CHEESEHEAD19 domain with markers indicating the flux tower locations.*

4 Methods

The model used in this research is based on the one described by Desai et al., who used a 1D forcing for ABL growth and advection over the domain with the mean wind. Since subsidence is not taken into account, there are two processes at play: the 1D surface forcing and the advection, which are described separately below.

4.1 Surface forcing

The simplest version of this model is 1-dimensional with the boundary layer only being forced by the surface buoyancy flux. Tennekes [1973] suggested a parameterization of the entrainment process, from which Batchvarova and Gryning [1991] derived a differential equation for the boundary layer height:

$$\Big\{\Big(\frac{h^2}{(1+2A)h-2B\kappa L}\Big)+\frac{Cu_*^2T}{\gamma g[(1+A)h-B\kappa L]}\Big\}\frac{dh}{dt}=\frac{B_s}{\gamma}, \tag{1}$$

where h is the ABL depth [m], A, B, C are a parameterization constants, κ is the von Kármán constant, L is the Obhukov length [m], u_* is the friction velocity [m/s], T is the near-surface temperature [K], γ is the virtual potential temperature gradient above h [K/m], g is the gravity [m/s^2] and B_s is the surface buoyancy flux [K m/s]. The first term on the left-hand side represents the combination of convective and mechanical turbulence and the second term stems from the spin-up effect. Mechanical turbulence and the spin-up of the system are only important in very early morning when the boundary layer is shallow [Batchvarova and Gryning, 1991]. Neglecting these terms ($B=0, C=0$), equation 1 reduces to

$$\frac{dh}{dt}=\frac{(1+2A)B_s}{h\gamma}. \tag{2}$$

The parameter A signifies the relative importance of entrainment at the top of the boundary layer and is usually assumed 0.2 [Tennekes, 1973]. Following Desai et al., the buoyancy flux B_s can be calculated from flux tower measurements of the sensible heat flux H_s and latent heat flux L_s using

$$B_s=\frac{H_s}{\rho c_p}+0.61\theta_s\Big(\frac{L_s}{\rho_d L_v}\Big), \tag{3}$$

where ρ, ρ_d are the density of air and density of dry air at the surface [kg/m^3], c_p is the specific heat of dry air [J/(kg K)] and L_v is the latent heat of evaporation [J/kg].

Using the flux measurements at all towers in the domain, equation 2 can be integrated in time from an initial condition to calculate the growth of the boundary layer during the day. By using observations of latent and sensible heat flux, the moisture and heat feedbacks described in section 2.1.1 are taken into account without modelling the actual processes.

4.2 Advection

Desai et al. used the 1D model equation described above and added an advection term to study the variability along a track, treating the ABL as a well-mixed fluid moving with the wind. The same approach is taken here, applying this principle to a 3D domain. The differential equation then becomes

$$\frac{\partial h}{\partial t}=\frac{(1+2A)B_s}{z_i\gamma}-u\frac{\partial h}{\delta x}-v\frac{\partial h}{\delta y}, \tag{4}$$

where u, v are the mean wind speeds in x and y direction, respectively [m/s].

Equation 4 can be integrated numerically using a second order Lax-Wendroff scheme with a timestep of 120 s or less. The buoyancy flux B_s calculated using equation 3 at the 17 Ameriflux towers and tall tower is regridded over the domain, using a grid size of 100 m and the cubic algorithm from the scipy toolbox [SciPy] after which the missing data is filled with the nearest neighbour. The footprints are not taken into account in this calculation, since these are typically on the scale of the grid size used in this model.

The model has periodic boundary conditions and is initialized homogeneously, using the balloon sounding profiles during the IOP's and a constant initial condition of 500 m for the rest of the period. The method used to find the BLH from balloon soundings is described below.

4.3 Inital condition

There are multiple methods to find the BLH from atmospheric profiles. Salcido et al. [2003] proposed a method called the Least-Squares Variational Approach (LSVA): the fitting of a theoretical ABL structure to a virtual potential temperature profile. He tested this method in [Salcido et al., 2020] against the parcel method, the gradients method and a covariance method. Since the LSVA method was considered to be applicable to more various and irregular profiles, this method was used here.

The LSVA method fits a theoretical profile $\overline{\theta}(z)$ to an observed profile $\theta(z)$ of virtual potential temperature (VPT). The theoretical profile has 3 sections: A mixing layer with constant VPT from the surface to the BLH h, a zero-thickness entrainment zone at $z = h$ where the VPT jumps from θ_m to θ_0 and lastly the free atmosphere $(z > h)$ where the VPT increases with height linearly with a slope γ. The equation describing this theoretical profile is

$$\overline{\theta}(z, h, \theta_m, \theta_0, \gamma) = \theta_m\big[1 - H(z-h)\big] + \big[\theta_0 + \gamma(z-h)\big]H(z-h), \tag{5}$$

where H is the heaviside function.

The scipy optimizing algorithm is then used to perform a least-squares fit of the observed profile to this theoretical one, optimizing all four parameters simultaneously: $\{h, \theta_m, \theta_0, \gamma\}$ by minimizing the following function

$$F(h, \theta_m, \theta_0, \gamma) = \int_a^b \Big[\overline{\theta}(z, h, \theta_m, \theta_0, \gamma) - \theta(z)\Big]^2 dz, \tag{6}$$

where a and b determine the height range to take into account. The choice of these parameters is important because the result is best if no other atmospheric layers are included. One addition was introduced compared to the method described by Salcido, namely inside the optimizing algorithm, equation 6 was multiplied by parabolic weights centered around h, so that the distance between the fit and observed profile were weighed stronger around the BLH while minimizing this distance. This addition significantly improved the fits. Two results of this method are shown in figure 3, with a morning profile on the left and afternoon profile on the right. Morning profiles are found to be generally less defined which makes the detection of the BLH less accurate. To initialize the model, these fits were checked and adjusted by eye if necessary.

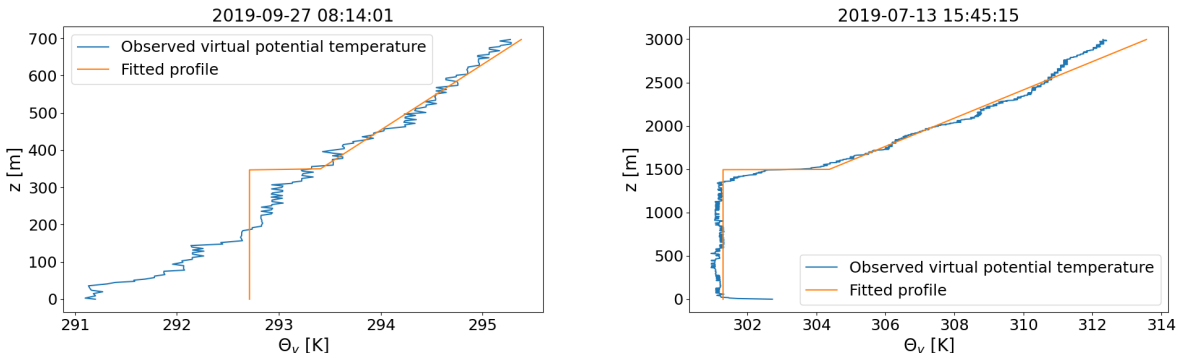

(a) (b)

Figure 3: *Observed profiles of virtual potential temperatures from balloon soundings, as well as the fitted profiles used to find the BLH.*

4.4 Testing

First of all, a test case is performed using a constant buoyancy flux in time, shown in figure 4a and wind speed of 5 m/s in North-East direction (45°). The final state of the model run with an initial state $h_0 = 500$ m and dt = 60 s is shown in figure 4b. This case is used to study the influence of the initial condition, running it for initial conditions $h_0 = [100, 500, 1000]$ m. In figure 5 the mean and standard deviation over the domain is shown for 1 day, with the initial condition subtracted from the mean. This figure shows that the initial condition has a large influence on the final state. Both the mean growth of the BLH and the spatial variance, shown as shading, are affected by the initial state. For a larger initial BLH, there is less growth and less spatial variance, so the solutions shown might have converged in a longer simulation. However, since the boundary layer goes through a diurnal cycle this is not applicable and the strong dependence on initial condition should be taken into account.

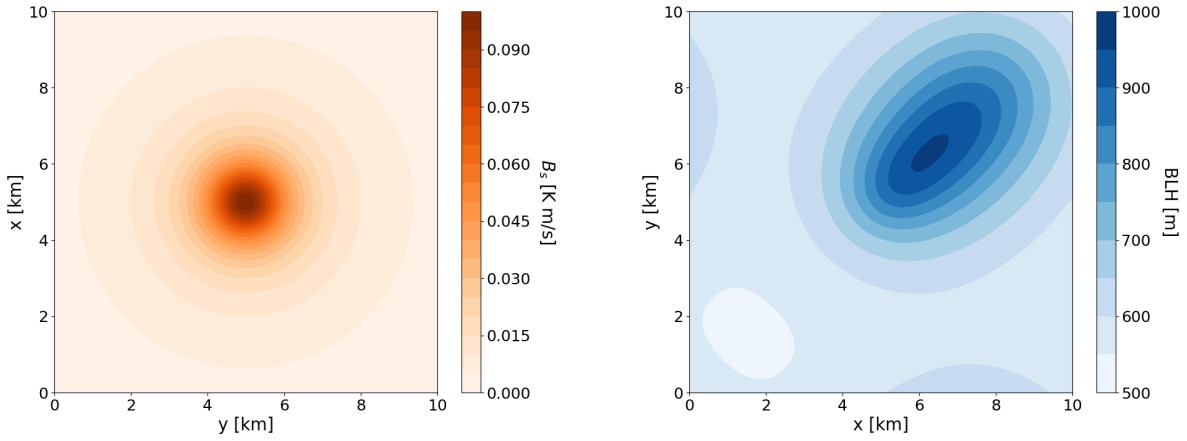

(a) (b)

Figure 4: *(a) Buoyancy flux map used for test case. (b) BLH final state of test case with a wind speed of 5 m/s in North-East direction (45°), initial BLH of 500 m and dt = 60 s.*

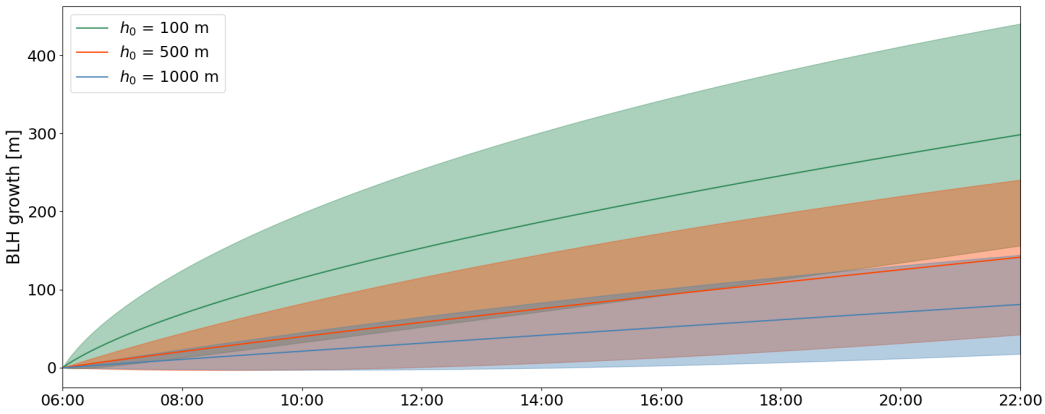

Figure 5: *Plot of BLH growth for different initial conditions, as well as spatial standard deviation, shown as shaded area.*

5 Results

The domain used for all the simulation was 10 km x 10 km and the South-West corner of the domain has coordinates (45.90, -90.35). In figure 6, the x-axis points East and the y-axis points North.

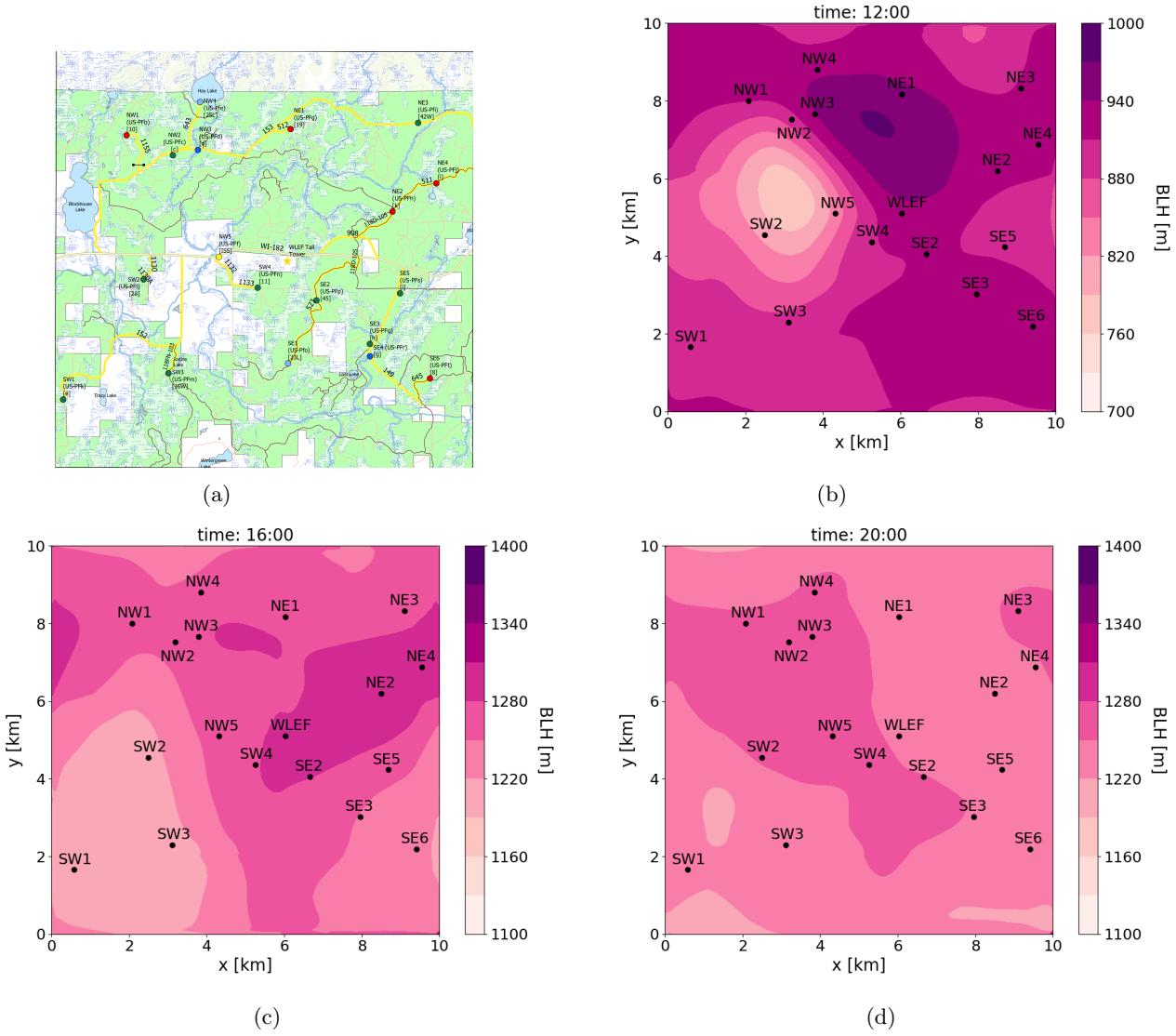

Figure 6: *(a) Map of CHEESEHEAD19 domain, same as figure 2. (b,c,d) Maps of BLH at 12:00, 16:00, 20:00, averaged over all IOP days.*

5.1 Spatial Patterns

As described in the theory section, surface properties have a strong influence on the forcing of the ABL growth, which is modelled here as the buoyancy flux. Figure 6b,c,d show the BLH simulated by the model at 3 times during the day, averaged over all IOP days. Figure 6a shows a map of the domain. The simulated BLH has heterogeneities that are consistent over the IOP's at noon, with a deep boundary layer in between NE1, NW3 and WLEF $[x = 5, y = 7]$ and relatively shallow boundary layer in between SW2, NW5 and NW2 $[x = 3, y = 5]$. The gradient between these two extremes in the domain is around 100 m BLH / km distance. These gradients occur because of heterogeneities in the bouyancy flux, and the short time from the beginning of the simulation, which means advection has not yet evened out the spatial differences. When the day progresses, the gradients

typically lessen as can be seen in figures 6c and 6d, which is a result of the mixing of BLH by advection.

5.2 BLH and Buoyancy Variability

To see how much the variance in buoyancy flux gets imprinted on the BLH in the model, simulations were also done for the full CHEESEHEAD19 study period, from mid June to mid October 2019. The spatial standard deviation of the BLH and the buoyancy flux was averaged daily and these results are shown in figure 7 for the simulations that excluded advection. In this figure the size of the markers represents the daily average buoyancy flux magnitude and the color represents the date.

Figure 7 shows that using just the 1D model and thereby neglecting all horizontal processes, the variance in buoyancy flux clearly translates into variance in BLH. The colors in this plot show that the earlier dates in the summer of 2019 had higher buoyancy variance and that over the summer this variance dropped. The size of the markers show that the earlier dates have higher buoyancy magnitude as well, so over the course of the summer both the buoyancy magnitude and spatial variability decreased. From this plot, a linear slope between BLH standard deviation and buoyancy flux standard deviation is found of $\alpha \approx 2700$ m/(K m/s).

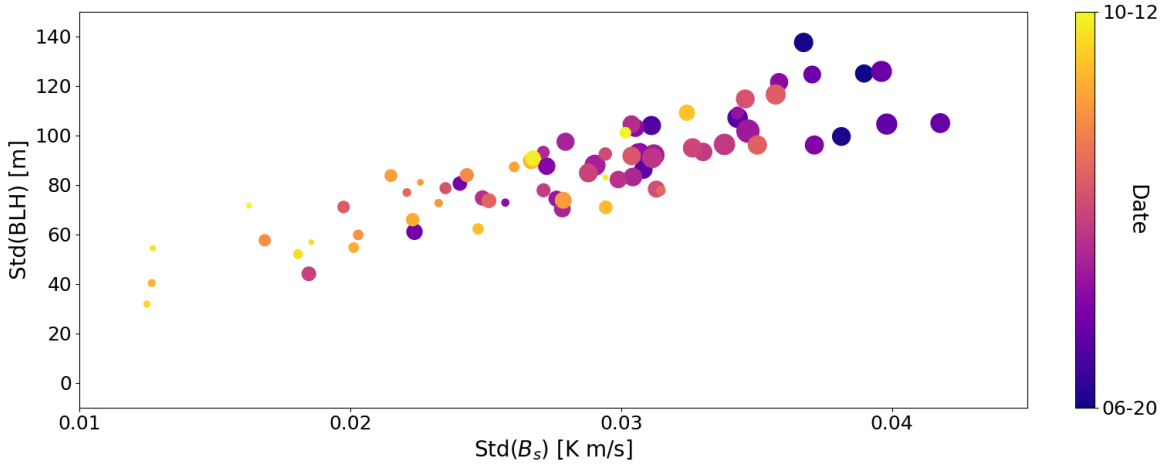

Figure 7: *Spatial standard deviation of BLH plotted against spatial standard deviation of surface buoyancy flux, for the simulations without advection. Data points are daily averages, the colors indicate the date and the size of the markers indicate the daily average magnitude of the buoyancy flux.*

In figure 8 the spatial standard deviations are shown for the simulations that included advection. In this figure, the size of the markers represent the daily average of the wind speed.

This figure shows the effect that advection of BLH has on the translation of buoyancy variability to BLH variability. By using the average wind data (shown as size of markers) this translation is dampened, as the larger markers mostly have low BLH variance. The clear linear relation visible in figure 7 is no longer present, but this figure suggests that buoyancy and BLH variability are still connected. For Std(B_s) < 0.025 K m/s, the relation seems to hold, while for larger buoyancy variance and larger wind speeds, the BLH variance no longer grows.

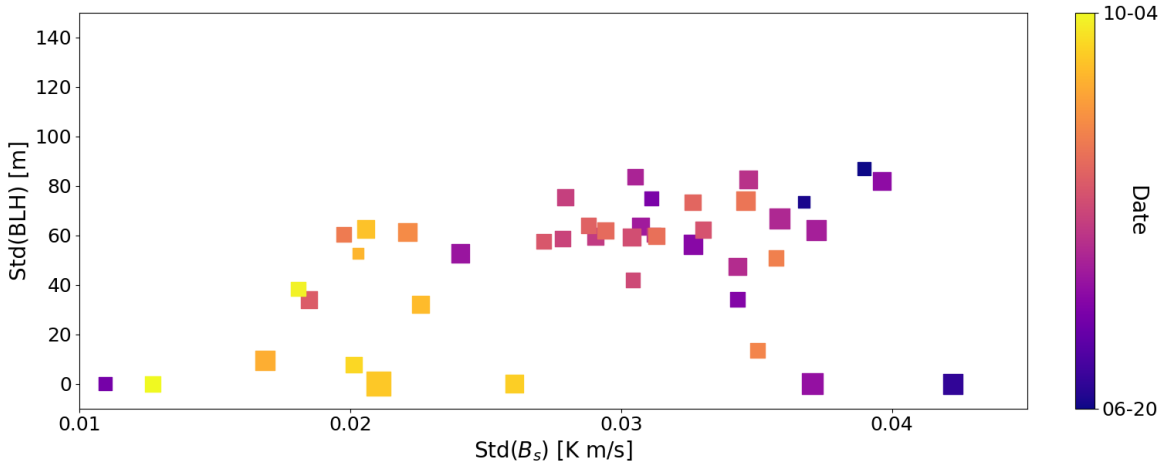

Figure 8: *Spatial standard deviation of BLH plotted against spatial standard deviation of surface buoyancy flux for the simulations with advection. Data points are daily averages, the colors indicate the date and the size of the markers indicate the daily average wind speed.*

5.3 IOP's

The balloon soundings done at NW5 (ISS) at 8:00 during the IOP's were used to initialize the model for those days. To find the BLH from the balloon sounding, the method described in section 4.3 is used. The result of these fits were checked by eye and adjusted when the fit was too far from the sounding profile. Figure 9 shows the results of these simulations, with the average BLH and its standard deviation over the domain in blue, as well as the average buoyancy flux and its standard deviation in red. Also, the conditions during the days, as evaluated by Sedlar et al. [2022], are shown as well as the average wind speed used for the advection scheme. Lastly, the BLH as calculated from the balloon soundings at 16:00 is shown as a green marker.

First of all, the BLH in IOP1 starts relatively high and has low spatial variability, seen from the blue shaded areas. This is in accord with the wind speeds that are relatively high. Also, the cloudy days have higher final BLH, which makes sense when considering that in theory clouds will form when air gets mixed to the height of the LCL. The green markers show that the balloon sounding observations are reasonably well reproduced by the model, with the cloudy days showing a larger discrepancy than the clear days. IOP2 shows lower BLH with higher spatial variability which is in accord with lower wind speeds. The three cloudy days in this period have a much lower simulated BLH than the balloon sounding observations, which are relatively high. In IOP3 the variability again is low and wind speeds are high. Here the clear and cloudy day balloon sounding observations are not far apart, but the model simulates a much lower BLH on the clear days than on the cloudy days. Over all three IOP's, the error between predicted and observed BLH is approximately 100 m on clear days and more than 500 m on cloudy days.

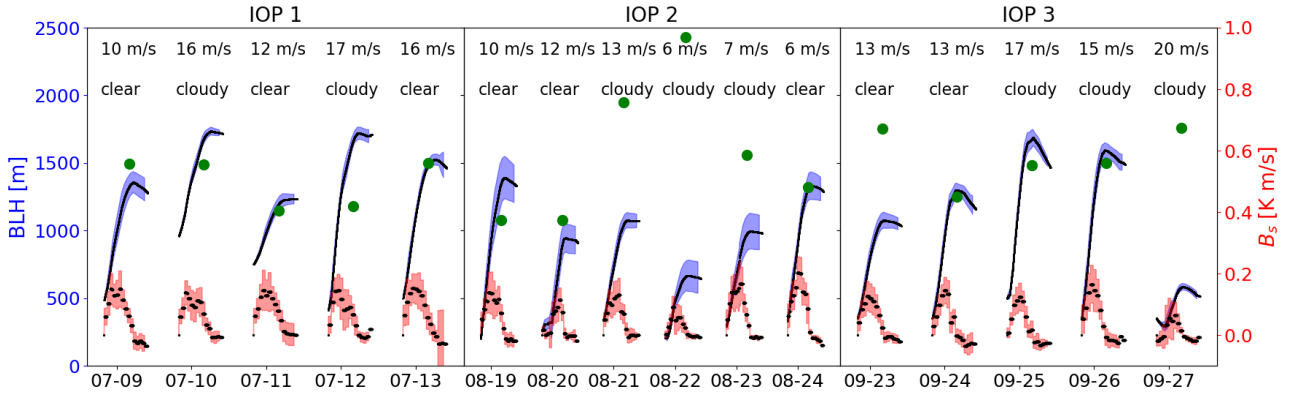

Figure 9: *BLH from simulations including advection plotted for the 3 IOP's, as well as the used buoyancy flux. Shaded areas indicate spatial standard deviation. The green dots are BLH's calculated from balloon soundings at 16:00 each day. Also shown is the mean wind speed and cloud conditions.*

6 Discussion

The model developed for this research produces realistic values of BLH. As was found by Desai et al. [2006], the initial atmospheric profile used has large influence on the BLH reached during the day, because the diurnal cycle is too short for the final state to become independent of the initial condition.

From the 1D model only taking into account surface forcing, heterogeneities in the observed surface buoyancy flux cause heterogeneities in the modelled BLH on the scale of 100 m. The spatial variance in buoyancy flux shows a clear correlation with the spatial variance in BLH. When using wind speed to advect the BLH, the BLH variance dropped. For the period considered here, the summer of 2019, there was still a correlation visible between the spatial variances of buoyancy flux and BLH. This could point to heterogeneities being imprinted on the boundary layer by the surface on smaller scales than were found by Desai et al. [2006], namely in the order of 1 km.

When comparing the model results with the cloud conditions as evaluated by Sedlar et al. [2022], on clear days the modelled BLH is closer to observations than on cloudy days, the errors being approximately 100 m and more than 500 m, respectively. Since cloudy days are associated with more instabilities, higher wind speeds and shear, this points to the model assumptions not holding for cloudy conditions. To obtain more accurate predictions, some processes in the system would have to be modelled more explicitly, entrainment being the most important process that changes for cloudy conditions [Edwards et al., 2020b]. Future research could include adding the cloud-feedback into this model, as was done by Konings et al. [2010] for example, to see if this would improve the results and if such a model could predict rainfall.

In general, the results that this model produces should be validated more extensively. Duncan Jr et al. [2022] recently evaluated the ability of a range of instrumentation used in the CHEESEHEAD19 study to estimate the BLH. Options for validation that they include are the radar wind profilers, microwave radiometers, atmospheric emitted radiance interferometers, ceilometers, high spectral resolution lidars and Doppler lidars. Also, it would be interesting to compare the results from this simple model to LES model results.

Several processes were neglected in this research. First of all, large-scale subsidence in the atmosphere was not taken into account. In Desai et al. [2006] this accounted for a reduction in BLH in the order of 100 m, but since this is a large scale process this would likely not have an effect on the spatial variability of the BLH. Also, in this study the footprints of the flux towers were not taken into account. Helbig et al. wrote in their review that researchers should be aware of a spatial mismatch between flux footprints and calculated BLH, especially when looking at site-specific applications. In this case the footprints were typically the same size as the grid cells, but if a higher resolution is used or more small-scale features are studied, this is something that could be

added to the regridding method.

7 Conclusion

A 1D advection-resolved model was developed to predict the BLH using observed buoyancy fluxes in the CHEESEHEAD19 domain. The first research was: Are surface heterogeneities imprinted on the BLH in the 'terra incognita' and what variables influence this process? The 1D model showed strong correlation between spatial variance in buoyancy flux and BLH. This correlation was weakened when adding advection, mixing the BLH horizontally using the mean wind. Stronger wind speeds were found to cause smaller BLH variability, in the order of 100 m on average over the domain.

The second research question was: How well does a 1D BLH model with a 2D advection scheme reproduce the BLH and does this depend on the cloud conditions? When the model was initialized with observed morning BLH from balloon soundings, the results were within 100 m from from observations for clear days and more than 500 m from observations for cloudy days. Since cloudy days are more likely to have stronger winds, wind shear and divergence, the model assumptions do not hold in these conditions, which causes the error between prediction and observation. To improve the model, subsidence should be added and the flux tower footprints could be used to create a more accurate spatial grid. The model should also be validated more extensively, using other available instrumentation or LES model results. To investigate cloud conditions, the cloud-moisture feedback could be added to this model to better predict BLH and perhaps rainfall.

References

Ekaterina Batchvarova and Sven-Erik Gryning. Applied model for the growth of the daytime mixed layer. *Boundary-Layer Meteorology*, 56(3):261–274, 1991.

Sandrine Bony and Jean-Louis Dufresne. Marine boundary layer clouds at the heart of tropical cloud feedback uncertainties in climate models. *Geophysical Research Letters*, 32(20), 2005.

Brian J Butterworth, Ankur R Desai, Stefan Metzger, Philip A Townsend, Mark D Schwartz, Grant W Petty, Matthias Mauder, Hannes Vogelmann, Christian G Andresen, Travis J Augustine, et al. Connecting land–atmosphere interactions to surface heterogeneity in cheesehead19. *Bulletin of the American Meteorological Society*, 102(2):E421–E445, 2021.

Ankur R Desai, Kenneth J Davis, Christoph J Senff, Syed Ismail, Edward V Browell, David R Stauffer, and Brian P Reen. A case study on the effects of heterogeneous soil moisture on mesoscale boundary-layer structure in the southern great plains, usa part i: Simple prognostic model. *Boundary-layer meteorology*, 119 (2):195–238, 2006.

James B Duncan Jr, Laura Bianco, Bianca Adler, Tyler Bell, Irina V Djalalova, Laura Riihimaki, Joseph Sedlar, Elizabeth N Smith, David D Turner, Timothy J Wagner, et al. Evaluating convective planetary boundary layer height estimations resolved by both active and passive remote sensing instruments during the cheesehead19 field campaign. *Atmospheric Measurement Techniques*, 15(8):2479–2502, 2022.

John M Edwards, Anton Beljaars, Albert AM Holtslag, and Adrian P Lock. Representation of boundary-layer processes in numerical weather prediction and climate models. *Boundary-Layer Meteorology*, 177(2):511–539, 2020a.

John M Edwards, Anton Beljaars, Albert AM Holtslag, and Adrian P Lock. Representation of boundary-layer processes in numerical weather prediction and climate models. *Boundary-Layer Meteorology*, 177(2):511–539, 2020b.

John Roy Garratt. The atmospheric boundary layer. *Earth-Science Reviews*, 37(1-2):89–134, 1994.

Tobias Gerken, Gabriel T Bromley, and Paul C Stoy. Surface moistening trends in the northern north american great plains increase the likelihood of convective initiation. *Journal of Hydrometeorology*, 19(1):227–244, 2018.

Manuel Helbig, Tobias Gerken, Eric R Beamesderfer, Dennis D Baldocchi, Tirtha Banerjee, Sébastien C Biraud, William OJ Brown, Nathaniel A Brunsell, Elizabeth A Burakowski, Sean P Burns, et al. Integrating continuous atmospheric boundary layer and tower-based flux measurements to advance understanding of land-atmosphere interactions. *Agricultural and Forest Meteorology*, 307:108509, 2021.

John C Kealy, Georgios A Efstathiou, and Robert J Beare. The onset of resolved boundary-layer turbulence at grey-zone resolutions. *Boundary-Layer Meteorology*, 171(1):31–52, 2019.

Alexandra G Konings, Gabriel G Katul, and Amilcare Porporato. The rainfall-no rainfall transition in a coupled land-convective atmosphere system. *Geophysical Research Letters*, 37(14), 2010.

Zhanqing Li, Jianping Guo, Aijun Ding, Hong Liao, Jianjun Liu, Yele Sun, Tijian Wang, Huiwen Xue, Hongsheng Zhang, and Bin Zhu. Aerosol and boundary-layer interactions and impact on air quality. *National Science Review*, 4(6):810–833, 2017.

AP Lock, AR Brown, MR Bush, GM Martin, and RNB Smith. A new boundary layer mixing scheme. part i: Scheme description and single-column model tests. *Monthly weather review*, 128(9):3187–3199, 2000.

Sebastiaan Luyssaert, Mathilde Jammet, Paul C Stoy, Stephan Estel, Julia Pongratz, Eric Ceschia, Galina Churkina, Axel Don, KarlHeinz Erb, Morgan Ferlicoq, et al. Land management and land-cover change have impacts of similar magnitude on surface temperature. *Nature Climate Change*, 4(5):389–393, 2014.

Amilcare Porporato. Atmospheric boundary-layer dynamics with constant bowen ratio. *Boundary-layer meteorology*, 132(2):227–240, 2009.

Andreas F Prein, Wolfgang Langhans, Giorgia Fosser, Andrew Ferrone, Nikolina Ban, Klaus Goergen, Michael Keller, Merja Tölle, Oliver Gutjahr, Frauke Feser, et al. A review on regional convection-permitting climate modeling: Demonstrations, prospects, and challenges. *Reviews of geophysics*, 53(2):323–361, 2015.

Alejandro Salcido, R Sozzi, and Telma Castro. Least squares variational approach to the convective mixing height estimation problem. *Environmental Modelling & Software*, 18(10):951–957, 2003.

Alejandro Salcido, Ana-Teresa Celada-Murillo, Susana Carreón-Sierra, Telma Castro, Oscar Peralta, Rogelio-Sebastián Salcido-González, Nicasio Hernández-Flores, Gustavo-Adolfo Tamayo-Flores, and Marco-Antonio Martínez-Flores. Estimations of the mexicali valley (mexico) mixing height. *Atmosphere*, 11(5):505, 2020.

Joseph A Santanello Jr, Christa D Peters-Lidard, and Sujay V Kumar. Diagnosing the sensitivity of local land–atmosphere coupling via the soil moisture–boundary layer interaction. *Journal of Hydrometeorology*, 12 (5):766–786, 2011.

SciPy. Scipy.interpolate.griddata. URL `https://docs.scipy.org/doc/scipy/reference/generated/scipy.interpolate.griddata.html`.

J Sedlar, LD Riihimaki, DD Turner, J Duncan, B Adler, L Bianco, K Lantz, J Wilczak, Emiel Hall, Christian Herrera, et al. Investigating the impacts of daytime boundary layer clouds on surface energy fluxes and boundary layer structure during cheesehead19. *Journal of Geophysical Research: Atmospheres*, 127(5): e2021JD036060, 2022.

Hendrik Tennekes. A model for the dynamics of the inversion above a convective boundary layer. *Journal of Atmospheric sciences*, 30(4):558–567, 1973.

Chiel C Van Heerwaarden, Jordi Vilà-Guerau de Arellano, Arnold F Moene, and Albert AM Holtslag. Interactions between dry-air entrainment, surface evaporation and convective boundary-layer development. *Quarterly Journal of the Royal Meteorological Society: A journal of the atmospheric sciences, applied meteorology and physical oceanography*, 135(642):1277–1291, 2009.

Elizabeth SK Vick, Paul C Stoy, Angela CI Tang, and Tobias Gerken. The surface-atmosphere exchange of carbon dioxide, water, and sensible heat across a dryland wheat-fallow rotation. *Agriculture, Ecosystems & Environment*, 232:129–140, 2016.

John C Wyngaard. Toward numerical modeling in the "terra incognita". *Journal of the atmospheric sciences*, 61(14):1816–1826, 2004.